

Tomographic Heating Holder for *In Situ* TEM: Study of Pt/C and PtPd/Al₂O₃ Catalysts as a Function of Temperature

Lionel C. Gontard,^{1,*} Rafal E. Dunin-Borkowski,² Asunción Fernández,¹ Dogan Ozkaya,³ and Takeshi Kasama⁴

¹Instituto de Ciencia de Materiales de Sevilla (CSIC), 41092, Sevilla, Spain

²Ernst Ruska-Centre for Microscopy and Spectroscopy with Electrons (ER-C) and Peter Grünberg Institute (PGI), Forschungszentrum Jülich, D-52425 Jülich, Germany

³Johnson Matthey Technology Centre, Blount's Court, Sonning Common, Reading RG4 9NH, UK

⁴Center for Electron Nanoscopy, Technical University of Denmark, DK-2800 Kgs. Lyngby, Denmark

Abstract: A tomographic heating holder for transmission electron microscopy that can be used to study supported catalysts at temperatures of up to ~1,500°C is described. The specimen is placed in direct thermal contact with a tungsten filament that is oriented perpendicular to the axis of the holder without using a support film, allowing tomographic image acquisition at high specimen tilt angles with minimum optical shadowing. We use the holder to illustrate the evolution of the active phases of Pt nanoparticles on carbon black and PtPd nanoparticles on γ -alumina with temperature. Particle size distributions and changes in active surface area are quantified from tilt series of images acquired after subjecting the specimens to increasing temperatures. The porosity of the alumina support and the sintering mechanisms of the catalysts are shown to depend on distance from the heating filament.

Key words: *in situ* TEM, TEM specimen holder, particle growth, heterogeneous catalysis, platinum, carbon black, platinum-palladium, alumina

INTRODUCTION

When studying heterogeneous catalysts, which frequently comprise metal nanoparticles on carbon black or an oxide support, an important goal is to observe the evolution of the active phase with temperature in the presence of reactant gases. Catalytic treatment can lead to changes in the surface area of the supported metal particles and hence catalytic activity due to processes such as sintering. In order to understand and control catalyst production, it is necessary to study how the dispersion and morphology of both the nanoparticles and the support depend on reaction conditions. Although phase diagrams of small metal particles have been proposed theoretically based on thermodynamics (Ajayan & Marks, 1988), they are incapable of predicting nanoparticle shapes that result from purely kinetic considerations. Recently, Barnard et al. (2009) proposed a quantitative phase map for gold nanoparticles based on *ab initio* calculations. However, a further complication is that such thermodynamic models do not take into account the role of the support, which determines the strength of attachment and thereby particle mobility and the possibility of phase transformations (Bett et al., 1974; Tauster, 1987; Sepúlveda-Escribano et al., 1998; González et al., 2009).

In situ transmission electron microscopy (TEM) refers to techniques that allow direct observation of dynamic properties at the nanoscale through imaging, spectroscopy, or diffraction. Such techniques can be used to understand the kinetics of phase transitions in heterogeneous catalysts and the importance of sintering mechanisms (Benavidez et al., 2010; Hansen et al., 2013). Possible approaches involve injecting gas directly into an environmental TEM (Hansen et al., 2002) and/or using dedicated sample holders that contain hot stages, gas or liquid cells, electrical contacts, fiber optics, and lasers for illuminating or heating the specimen while images are acquired with atomic spatial resolution (Kamino et al., 2005; Creemer et al., 2010; Cavalca et al., 2012; Mehraeen et al., 2013). *In situ* experiments that have made use of such instrumentation are nowadays common. Recent results have included studies of the role of promoters in Ru-based heterogeneous catalysts (Hansen et al., 2002), the oxidation of In, the reoxidation of Si and the formation of graphene on MgO-supported Pt nanoparticles (Kamino et al., 2005; Peng et al., 2012), as well as photodegradation of Cu₂O and photodeposition of Pt on a GaN:ZnO photocatalyst (Cavalca et al., 2012).

Here, we describe a TEM specimen holder that provides direct contact between a specimen and a filament that has a small thermal mass. The filament reaches a temperature that depends on the current flowing through it. There is then no need to use a support film, which can prevent effective thermal transfer and degrade image resolution. Kamino et al. (2005)

developed a similar specimen holder, which was equipped with a longitudinal tungsten wire aligned parallel to the rotation axis of the holder. In contrast, the filament in our holder is oriented perpendicular to the holder axis and has a narrow design, permitting acquisition of images at high specimen tilt angles ($\pm 80^\circ$) with minimal optical shadowing. This capability allows electron tomography to be used to analyze heterogeneous catalysts in three dimensions in combination with high temperature heating experiments.

We demonstrate the functionality of the holder by imaging the growth of Pt catalyst nanoparticles on carbon black *in situ* in the TEM as a function of temperature and by measuring the resulting changes in particle size distribution (PSD) and surface area of the active phase. We also study the formation of bimetallic PtPd particles on γ -Al₂O₃ and use high-angle annular dark-field (HAADF) scanning TEM (STEM) (Gontard et al., 2008, 2009) to obtain three-dimensional information about the porosity of the support after successive heat treatments.

MATERIALS AND METHODS

Tomographic Heating Holder

The tomographic specimen holder that we describe here contains a prewound tungsten filament taken from a light bulb (Fig. 1). We mount the filament in a removable cartridge, which is clamped onto two electrical contact pads in a specimen holder from E.A. Fischione Instruments Inc.

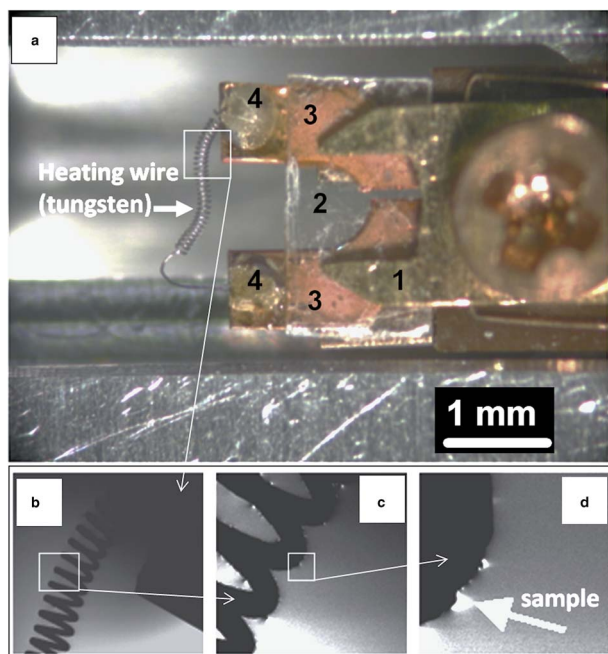


Figure 1. a: Modified TEM specimen holder with tungsten heating filament oriented perpendicular to the holder axis. The numbers correspond to (1) the clamp; (2) an insulating mica sheet; (3) Cu electric contacts; (4) silver epoxy resin. b–d: Three magnified images of the filament. The large arrow in (d) indicates an aggregate of the deposited specimen.

(Export, PA, USA). We glue the filament onto two pieces of a copper grid using silver epoxy and place a thin electrically insulating sheet of mica between the copper and the clamp.

Samples can be deposited directly onto the wire, either in the form of a dry powder or from solution. The ends of the wire, which has an electrical resistance of $\sim 5 \Omega$ and can be replaced between experiments if required, can be accessed electrically from outside the microscope. The wire temperature, which can be calibrated using an optical pyrometer before insertion into the TEM column, proved to be highly reproducible between different filaments. For example, a temperature of $\sim 1,000^\circ\text{C}$ was achieved by passing a current of $\sim 90 \text{ mA}$ through the wire. When operated in high vacuum, the filaments were typically found to fail at currents of $\sim 220 \text{ mA}$, corresponding to a temperature of just over $1,500^\circ\text{C}$. Tungsten wire has high thermo-mechanical stiffness and therefore does not sag significantly at high temperature, as well as a high melting point of $3,422^\circ\text{C}$ and a low vapor pressure. Experiments were performed with filaments operated for up to 12 h at currents of up to 150 mA (corresponding to a temperature of $\sim 1,300^\circ\text{C}$) with no significant signs of tungsten evaporation.

Pt Supported on Carbon Black

Pt particles with high dispersions ($>75 \text{ m}^2/\text{g}$), which were supported on mesoporous high-surface-area carbon blacks (Vulcan XC-72R) Pt (19.1 wt.%) and had been reduced in a N₂ atmosphere at 900°C , were provided by the Johnson Matthey Technology Centre in the form of a dry powder (Ralph & Hogarth, 2002; Ozkaya et al., 2003). The samples are used in proton exchange membrane fuel cells, which require high loadings of electrocatalysts. A small amount of powder that had been stored in air was placed directly onto the filament of the heating holder, inserted into a Philips (Eindhoven, The Netherlands) CM300 TEM operated at 300 keV , and reheated *in situ* by passing a current through the filament. The temperature was gradually increased from room temperature to 975°C in steps of either 25 or 50°C , allowing the specimen to stabilize between each step before acquiring a bright-field (BF) TEM image. Measurements of PSDs from the recorded images were obtained using dedicated image processing software based on adaptive segmentation (Gontard et al., 2011).

PtPd Supported on Alumina

PtPd nanoparticle formation was studied *in situ* in the TEM, starting from a dry powder of the precursor (Pt (HN3)₄)₂ Pd₂(EDTA) 2.5 wt.% on γ -Al₂O₃ (SFC-140). γ -Al₂O₃ is a metastable polytype of Al₂O₃, which is used extensively as a catalytic support material because of its high porosity and large surface area. In the present specimen, the formation of PtPd particles was expected to occur at temperatures of between 600 and 850°C . The experimental procedure was as follows: (1) The powder was placed onto the filament of the heating holder and inserted into an FEI (Eindhoven, The Netherlands) Tecnai F20 TEM. A region of the

specimen that could be tilted to high angles without shadowing was identified. A tilt series of HAADF STEM images of the region of interest was acquired at low magnification over a specimen tilt range of -52° to $+42^\circ$ using a 4° tilt increment; (2) *In situ* heating was performed in a Philips CM300 TEM, with the temperature of the filament increased from 500 to 850°C, allowing the specimen to equilibrate between steps. BF TEM images were acquired from the same area at high magnification at each temperature; (3) The specimen was allowed to cool to room temperature, the holder was reinserted into the Tecnai F20 TEM, and a new tilt series of HAADF STEM images was acquired from the same area. Alignment and tomographic reconstruction using the simultaneous iterative reconstruction technique were carried out using *Inspect3D* software (15–20 iterations). Voltex visualization of the final reconstructions was performed using *Amira V2.3* software. PSDs were measured using image processing software based on adaptive segmentation (Gontard et al., 2011).

RESULTS

Sintering of Pt Particles on C

Figure 2 shows a series of BF TEM images, which illustrate the sintering of Pt particles supported on carbon black during *in situ* heating at increasing temperature. Even though the specimen had already been reduced in an inert atmosphere at high temperature, Figure 2 shows that re-sintering occurs during heating in high vacuum, beginning at $\sim 550^\circ\text{C}$, accelerating between 650 and 850°C, and appearing to stop at 850°C. Faceting of the particles can then be seen, particularly for several larger particles. The shape of the C support does not change appreciably during sintering, although it rotates and translates within the field-of-view. In Figures 3a and 3b, circles and arrows are used to highlight differences between the same particles viewed at 500 and 925°C.

Figure 4 shows PSDs of the nanoparticles measured from selected images in Figure 2. Several statistical parameters are plotted, including mean size, standard deviation

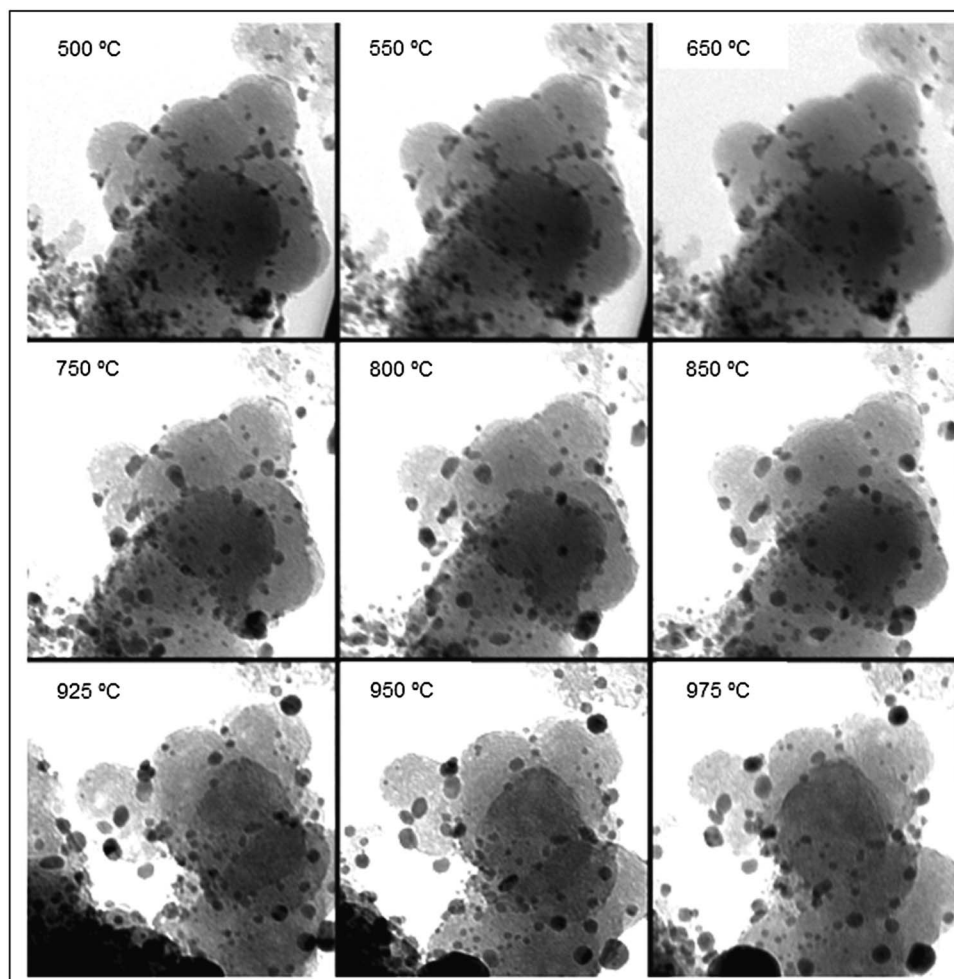


Figure 2. Series of bright-field transmission electron microscopy (BF TEM) images showing sintering of Pt nanoparticles on a carbon black support as a function of temperature between 500 and 975°C. The specimen was deposited directly onto the tungsten filament in the modified side-entry TEM specimen holder shown in Figure 1. The dark contrast at the bottom left corner of the images acquired at 925 and 950°C arises from the closest part of the filament to the region of interest.

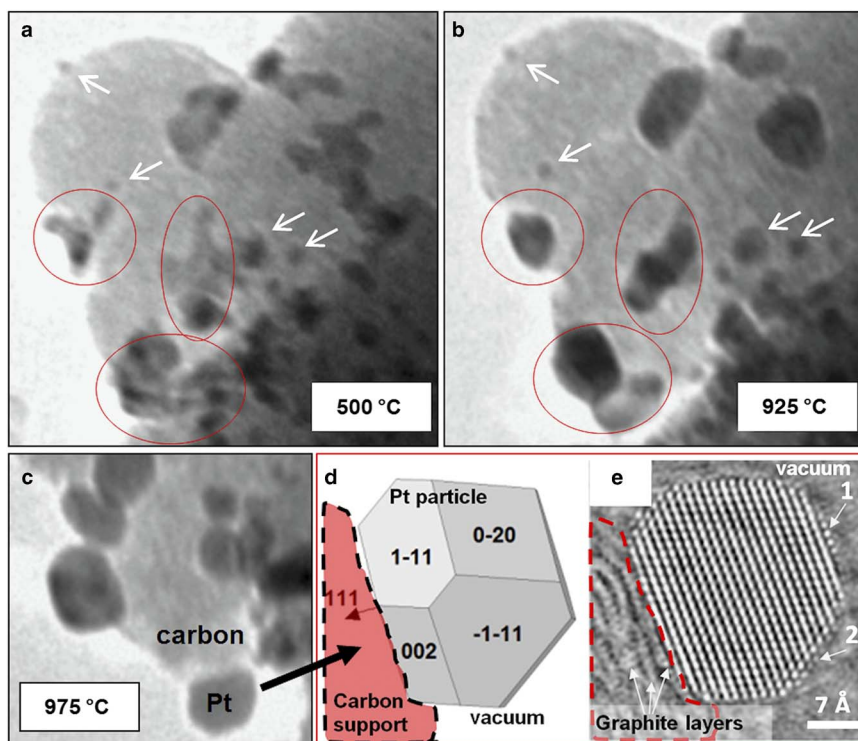


Figure 3. **a–b:** Detail extracted from the bright-field transmission electron microscopy (BF TEM) images shown in Figure 2, illustrating the coalescence of Pt nanoparticles between indicated specimen temperatures of 500 and 925°C. Red circles in both images show the initial and final configurations of selected Pt particles that have coalesced. White arrows indicate particles that remained strongly attached to the support and experienced smaller changes in their size. **c:** Detail of the attachment of a faceted Pt nanoparticle to the support. **d:** Model showing crystalline facets and possible Pt(111) contact plane of a Pt nanoparticle such as that shown in (e). **e:** Experimental high-resolution TEM image of one Pt particle on graphitized carbon (recorded from a similar specimen) showing atomic defects present at the surfaces (arrows 1 and 2) (Gontard et al., 2007).

and maximum size, for five selected temperatures (500, 650, 725, 875, and 950°C). The mean particle size was used to estimate the active surface area S_{area} . This is an important quantity in catalysis, as it describes the surface area of the active phase that is exposed to gases and can be used to understand catalyst deactivation. We made two approximations: (1) That the contact surface of the nanoparticles with the support is exposed to the gas; and (2) that the particles have spherical shapes with radii r_i . The surface area is then simply given by the expression

$$S_{\text{area}} = \sum_i^N \frac{s_i}{m_i} = \sum_i^N \frac{4\pi r_i^2}{\rho \cdot \frac{4}{3}\pi r_i^3} = \sum_i^N \frac{3}{\rho \cdot r_i},$$

where N is the number of particles, s_i and m_i are the surface area and mass of particle i and ρ is the density of Pt (i.e., 21.450 kg/m³). Figure 5 shows measurements of the evolution of S_{area} with temperature. The rate of loss of active area calculated from the slope of a linear fit, i.e., dS_{area}/dT is $-9 \times 10^3 \text{ m}^2/\text{kg}^\circ\text{C}$.

Formation of PtPd particles

Figure 6a shows TEM images of the precursor (Pt (HN₃)₄)₂ Pd₂(EDTA) 2.5 wt.% on γ -Al₂O₃ (SFC-140) recorded at

room temperature. Figure 6b shows an image of the same region of the specimen recorded after heating at 850°C. The images on the left side of the figure are HAADF STEM images, in which the local intensity is sensitive to atomic number (brighter regions correspond to particles). The BF TEM images shown in the right column of Figure 6 were acquired from the regions marked using rectangles in the left column. The images show that the PtPd particles grow at high temperature and that the γ -alumina support increases in porosity. Figure 6c shows the measured PSDs of the PtPd nanoparticles.

Figure 7 shows individual HAADF STEM images recorded at different specimen tilt angles from the same area of the alumina sample before and after heating, taken from a tilt series of images used for electron tomography. Figure 8a shows a vortex visualization of the three-dimensional reconstruction of this region of the specimen after heating, while Figure 8b shows an orthoslice generated from the reconstructed volume. Although the tilt step of 4° used for acquisition of the tilt series is relatively large and reduces the spatial resolution of the reconstructed volume, this value was chosen to minimize the total electron dose on the specimen. For example, it has been observed on samples of Pd supported on alumina that under electron irradiation Al₂O₃ can be

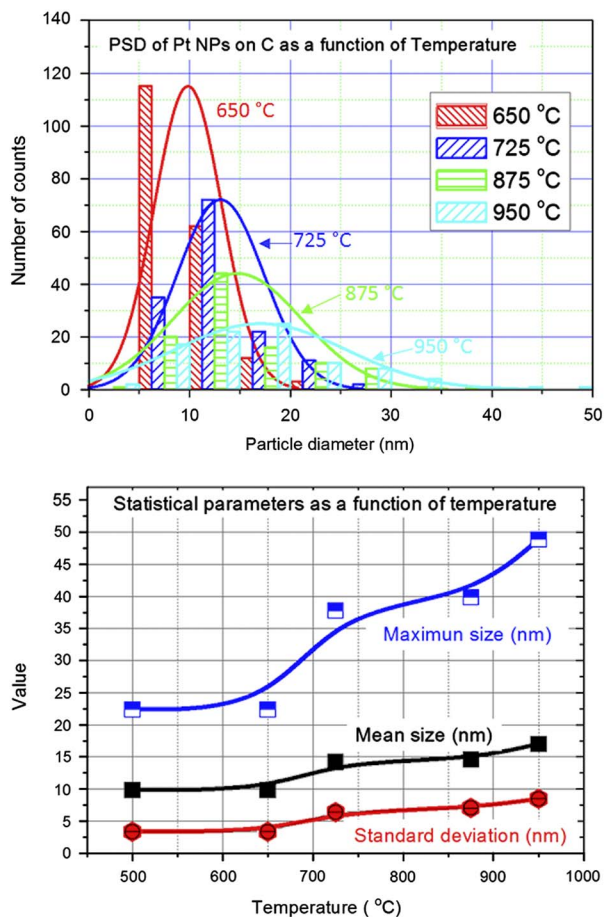


Figure 4. Top: particle size distributions (PSDs) of the Pt particles shown in Figures 2 and 3 measured at five selected temperatures between 650 and 950°C fitted with lognormal curves. Bottom: dependence of several statistical parameters (mean size, standard deviation and maximum size) on temperature. The values increase with temperature because of particle sintering.

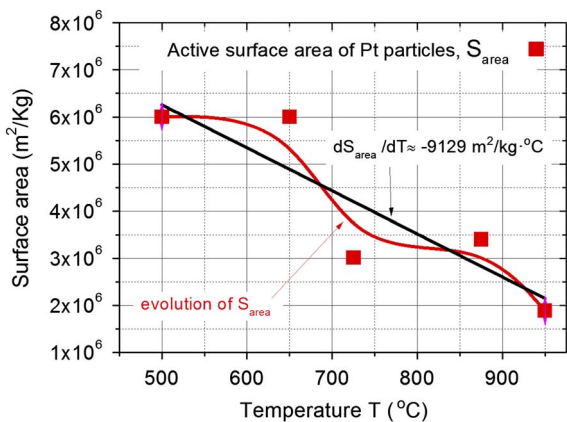


Figure 5. Active surface area of the Pt particles described in Figures 2–4, measured at five selected temperatures between 650 and 950°C (see text for details). Although the evolution of surface area is not linear we used the slope of a linear approximation as an estimate of the rate of loss of active surface area.

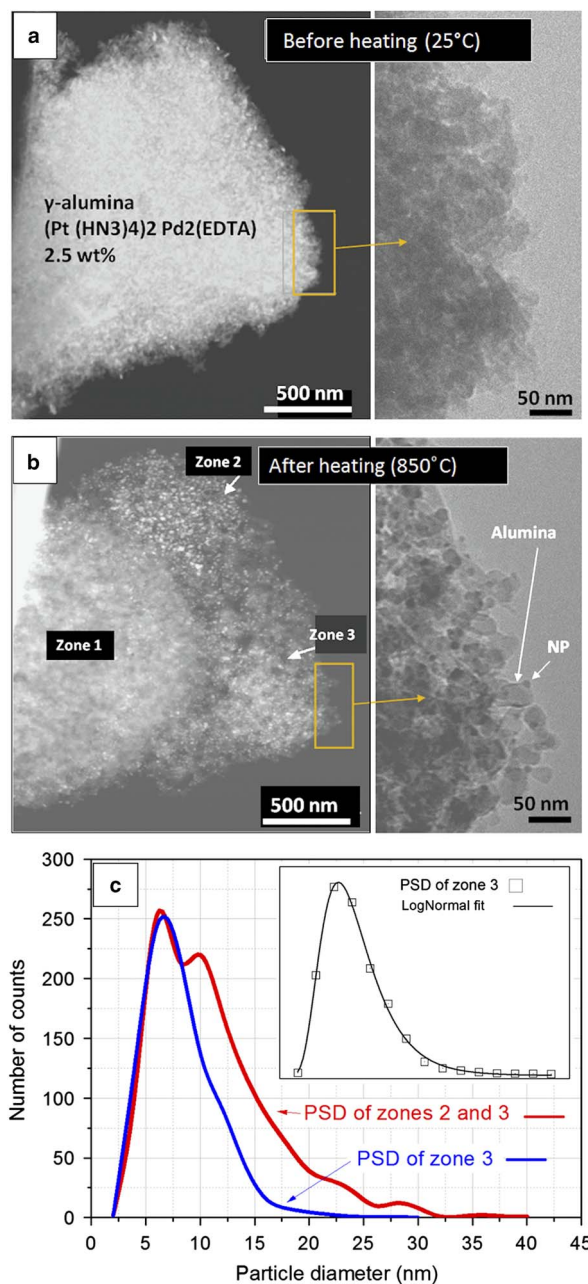


Figure 6. a–b: Annular dark-field scanning TEM (ADF STEM) images (left) and bright-field transmission electron microscopy (BF TEM) images (right) of (Pt(HN₃)₄)₂Pd₂(EDTA) 2.5 wt.% on γ -Al₂O₃ acquired (a) at room temperature (using the Tecnai F20) and (b) after increasing the temperature to 850°C (using the Philips CM300) in high vacuum conditions. The PtPd particle size and the porosity of the alumina differ between the marked zones. c: PSDs measured from zones 2 and 3 and from zone 3 alone, illustrating the formation of two families of particles with different average sizes.

reduced and a metastable intermetallic compound of Al₂Pd can form (Kamino et al., 1992). In the present experiments, the tilt range used was smaller than the maximum range that the holder allows ($\pm 80^\circ$), which also affects the quality of the final reconstruction, in particular in the z direction.

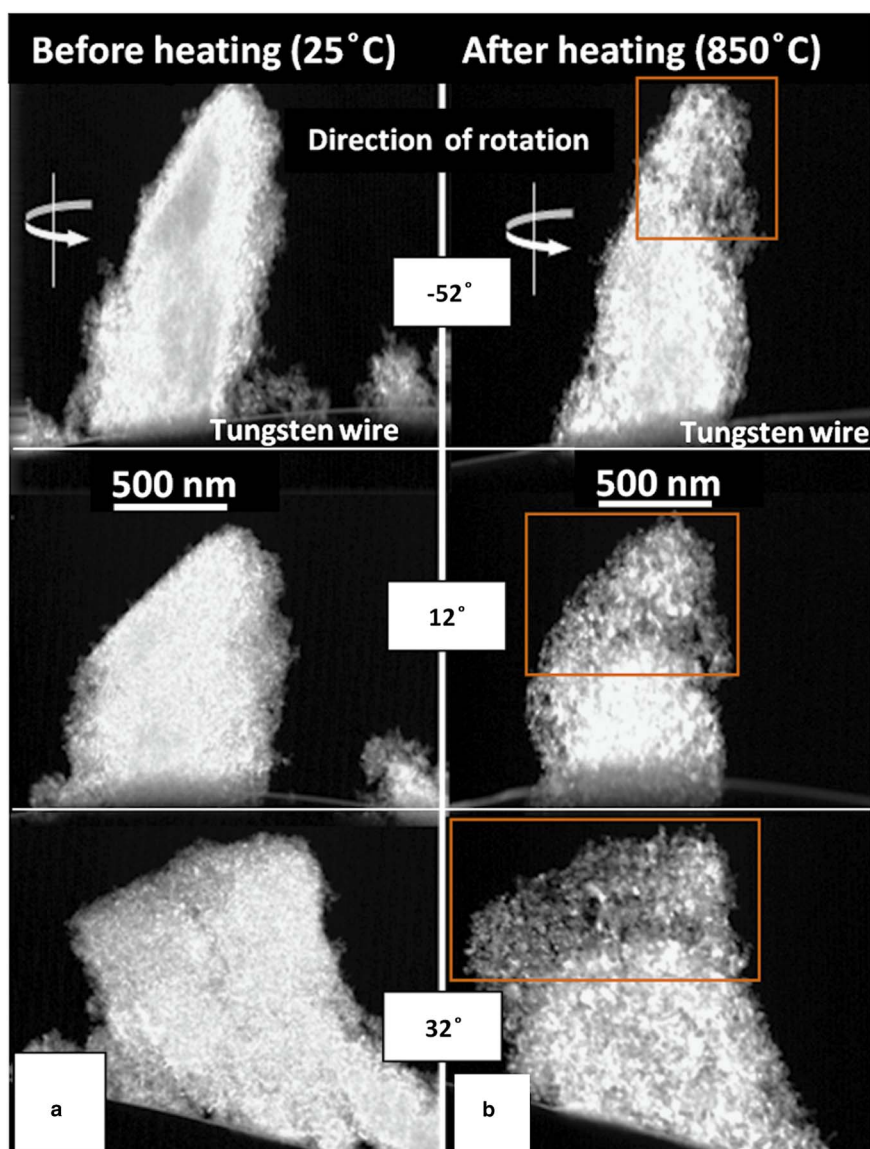


Figure 7. High-angle annular dark-field scanning TEM (HAADF STEM) images acquired from tomographic tilt series of the area of the sample of PtPd and alumina shown in Figure 6, (a) at room temperature (b) after heating the sample *in situ* to 850°C in high vacuum conditions using a Tecnai F20 TEM. The rectangles indicate the area used for tomographic visualization in Figure 8.

DISCUSSION

The results shown in Figures 2 to 8 can be used to discuss the *kinetic* route that catalyst nanoparticles follow when they grow on a specific support and to determine the relative importance of different sintering mechanisms (Benavidez et al., 2010; Hansen et al., 2013). Three possible sintering mechanisms are: (1) *Coalescence*, involving motion of the particles over the support and fusion (Ruckenstein & Lee, 1984). In general, at temperatures of $0.5 \times$ the melting point, metallic particles are expected to be in a quasi-melted state (continuously fluctuating between different structures), which favors coalescence (Ajayan & Marks, 1988; Barnard et al., 2009). (2) *Ostwald ripening*, involving the migration of individual atoms from the particles onto the support, across

the support, and onto other particles (Simonsen et al., 2010). Ostwald ripening is strongly dependent on atomic diffusivity (Linderoth et al., 1997; Horch et al., 1999) and can also happen in faceted particles in the form of *inhibited nucleation*, which arises from nucleation constraints and leads to slower growth rates than predicted by classical ripening theories (Wynblatt, 1976; Wynblatt & Gjostein, 1976); (3) An extension of Ostwald ripening, involving interparticle transport *via* a volatile oxide species (Harris, 1995; Ahn et al., 1981).

The curves in Figure 4 show directly that the rate of sintering of Pt particles on carbon black changes with temperature. The melting temperature of Pt particles is $\sim 884^\circ\text{C}$ (the melting temperature of bulk Pt is $1,768^\circ\text{C}$), which is much higher than the temperature at which the particles start to coalesce in our experiments. Figures 2 and 3 show

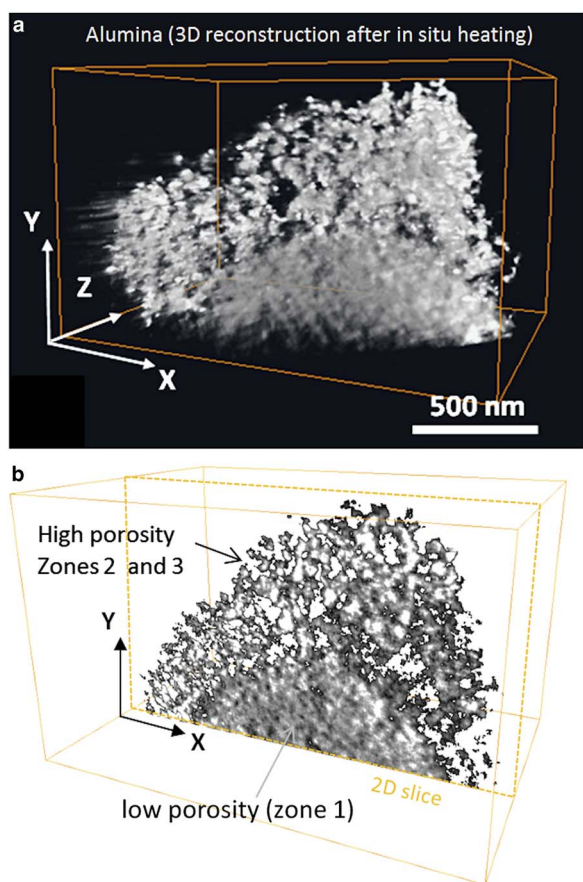


Figure 8. **a:** Voltex visualization of a tomographic reconstruction of the PtPd/alumina sample after in situ heating to 850°C in high vacuum conditions. The porosity is greater at the edge of the sample, far from the contact with the tungsten filament. **b:** Orthoslice visualization. Zone 1 (closer to the tungsten filament) is thought to be more compact than zones 2 and 3 as a result of transformation to α -alumina.

that particles or aggregates of particles that are close to each other or in contact coalesce and fuse between 600 and 725°C (circles in Figs. 3a, 3b), perhaps as a result of surface melting or premelting, involving the formation of quasi-liquid films on crystalline surfaces below the melting temperature (Ercoleso et al., 1991). High-resolution TEM studies have shown that the coalescence of gold particles begins with nanoparticle contact, followed by alignment of the coalescing planes at the interface between the nanoparticles. Liquid-like mobility of the nanoparticle surface layers (surface melting) is essential for this process to take place (José-Yacamán et al., 2005). The heat released during coalescence may result in subsequent melting of the entire particle. Surface melting also reduces surface tension, which favors particle diffusion, ripening, vapor formation and subsequent growth. As the Pt/C specimen studied here was not kept in vacuum before inserting it into the TEM, it is likely that some Pt oxides had formed during storage and then evaporated during the heating experiment, contributing to interparticle transport in the gas phase. The curves in Figure 4 show that the growth rate of the particles decreases at temperatures between 725

and 875°C. At these temperatures, most of the particles that were originally close to each other had fused into larger faceted particles (Figs. 2, 3). Growth rate deceleration is then also expected because nucleation-inhibited growth becomes important for faceted particles. The arrows in Figure 3a and 3b indicate particles that were initially isolated on the support. These particles are attached strongly to the support and grow when they are heated without moving from their original locations, presumably by Ostwald ripening (see Figs. 3c–3e). Strong adhesion to the support is expected because carbon black is composed of crystallites, in which many defects can occur on heating to high temperatures (Heidenreich et al., 1968; Coloma et al., 1995). Defects such as dislocations at the edges of planar domains of the graphitic layers may act as trapping sites for Pt nucleation (Bett et al., 1974), while surface defects on the particles can favor anchoring (Gontard et al., 2007). The curves in Figure 4 also show that above 875°C there is a further increase in the growth rate of the particles, which is not obvious from the images in Figure 2. Interestingly, this additional growth happens at a temperature close to 884°C, which is the expected melting temperature of Pt particles.

Phenomena taking place during the heating of Pt and Pd on alumina may be very different from those involving a pure Pt catalyst. For example, molecular dynamics simulations predict that, while at low temperature a PtPd nanoparticle has a core rich in Pt surrounded by a layer enriched in Pd, at the melting temperature Pt may diffuse to the surface (Sankaranarayanan, et al., 2005; Guisbiers et al., 2011). This redistribution of metal is important because heating experiments performed on PtPd particles supported on alumina have shown preferential loss of one of the active components from the catalyst (Pt or Pd) due to the presence of oxygen and differences in the vapor pressures of Pt and Pd oxides (Harris, 1986). In our experiment, we assume that the composition of the small particles that form at 850°C (see Fig. 6b) is PtPd, because preferential loss is not expected in these samples in *vacuum* at temperatures below 1,100°C (Clark et al., 1980; 1982). In future experiments, we plan to perform chemical characterization *in situ* using energy-dispersive X-ray spectroscopy. Figure 6b shows that porosity of the alumina support changed dramatically after heating. Interestingly, the degree of porosity changes locally across the sample and is related to the mean size achieved by the particles. The combined PSD of zones 2 and 3 in Figure 6c is multimodal with at least three maxima, while the PSD of zone 3 alone (inset in Fig. 6c) has a log-normal distribution with a single maximum. As the temperature approaches 1,000°C, the original γ - Al_2O_3 phase is expected to transform into thermodynamically-stable α - Al_2O_3 (corundum), while its surface area gradually decreases. The porosity of the alumina increases with temperature (its surface area increases) on the side of the sample that is furthest from the filament (zones 2 and 3), suggesting that the transition to the α - Al_2O_3 phase is unlikely to have happened in these zones. Figure 6b shows that the alumina close to the tungsten filament (zone 1) has lower porosity and hence may have started to transform to α -alumina. As the α - Al_2O_3 phase is refractory, a

decrease in heat conduction to the edge of the sample may then be expected, suggesting that not only the temperature but also the rate of heat flow is important for appropriate catalyst synthesis. The multimodal PSD shown in Figure 6 may therefore result from different temperatures having been reached in different parts of the alumina support.

SUMMARY

We have described a heating TEM specimen holder with a design that is optimized for the acquisition of tomographic series of images. The holder permits direct thermal contact between a specimen and a tungsten filament, which can reach temperatures above 1,000°C. Although the temperature of the filament is well-defined, the true temperatures of supported particles can depend on their size, on the nature of the substrate and their contact to it, on their distance from the filament, and on the current and current density of the electron beam (Mishra et al., 2010).

We tested the functionality of the holder by studying two heterogeneous catalyst systems. Pt particles on carbon black were found to be strongly attached to the carbon support. Above 600°C, the growth of the particles increased, mainly as a result of the coalescence of nearby particles, with smaller isolated particles growing slowly, most likely by Ostwald ripening. The formation of PtPd nanoparticles on alumina from a precursor was studied at temperatures of up to 850°C using electron tomography, including transformations of the alumina support with temperature. The tilt series, which were acquired here using a lower tilt range than the holder allows ($\pm 80^\circ$) and therefore with limited spatial resolution, revealed a strong variation in the porosity of the alumina and a multimodal PtPd PSD. The differences in porosity are likely to be associated with the presence of different phases (γ and α) of the alumina support, which have different thermal conductivity properties, at different distances from the heating element. Our observations demonstrate that not only the temperature but also the rate of heat flow across the catalyst support is important for appropriate nanoparticle synthesis.

ACKNOWLEDGMENTS

We are grateful to the European project REGPOT-CT-2011-285895-AI-NANOFUNC and to the European Union under a contract for an Integrated Infrastructure Initiative 312483 – ESTEEM2 funding and to Lionel Matsuya and Alan C. Robins for valuable contributions to this work.

REFERENCES

- AHN, T.M., WYNBLATT, P. & TIEN, J.K. (1981). Coarsening kinetics of platinum particles on oxide substrates. *Acta Metall* **29**, 921–929.
- AJAYAN, P.M. & MARKS, L.D. (1988). Quasimelting and phases of small particles. *Phys Rev Lett* **60**, 585–587.
- BARNARD, A.S., YOUNG, N.P., KIRKLAND, A.I., VAN HUIS, M.A. & XU, H. (2009). Nanogold: A quantitative phase map. *ACS Nano* **3**(6), 1431–1436.
- BENAVIDEZ, A.D., KOVARIK, L., GENÇ, A., AGRAWAL, N., LARSSON, E.M., HANSEN, T.W., KARIM, A.M. & DATYE, A.K. (2010). Environmental transmission electron microscopy study of the origins of anomalous particle size distributions in supported metal catalysts. *ACS Catal* **2**, 2349–2356.
- BETT, J.A., KINOSHITA, K. & STONEHART, P. (1974). Crystallite growth of platinum dispersed on graphitized carbon black. *J Catal* **35**, 307–316.
- CAVALCA, F., LAURSEN, A.B., KARDYNAL, B.E., DUNIN-BORKOWSKI, R.E., DAHL, S., WAGNER, J.B. & HANSEN, T.W. (2012). In-situ transmission electron microscopy of light-induced photocatalytic reactions. *Nanotechnology* **23**, 075705.
- CLARK, R.W., TIEN, J.K. & WYNBLATT, P. (1980). Loss of palladium from model platinum-palladium supported catalysts during annealing. *J Catal* **61**, 15–18.
- CLARK, R.W., WYNBLATT, P. & TIEN, J.K. (1982). Coarsening kinetics of alloy platinum-palladium particles on oxide substrates. *Acta Metall* **30**, 136–146.
- COLOMA, F., SEPÚLVEDA-ESCRIBANO, A. & RODRÍGUEZ-REINOSO, F. (1995). Heat-treated carbon blacks as supports for platinum catalysts. *J Catal* **154**, 299–305.
- CREEMER, J.F., HELVEG, S., KOOYMAN, P.J., MOLENBROEK, A.M., ZANDBERGEN, H.W. & SARRO, P.M. (2010). A MEMS reactor for atomic-scale microscopy of nanomaterials under industrially relevant conditions. *J Microelectromech Syst* **19**, 254–264.
- ERCOLESI, F., ANDREONI, W. & TOSATTI, E. (1991). Melting of small gold particles: mechanisms and size effects. *Phys Rev Lett* **66**(7), 911–914.
- GONTARD, L.C., CHANG, L.Y., HETHERINGTON, C.J.D., KIRKLAND, A.I., OZKAYA, D. & DUNIN-BORKOWSKI, R.E. (2007). Aberration-corrected imaging of active sites on industrial catalyst nanoparticles. *Angew Chem Int Ed* **46**, 3683–3685.
- GONTARD, L.C., DUNIN-BORKOWSKI, R.E. & OZKAYA, D. (2008). Three-dimensional shapes and spatial distributions of Pt and PtCr catalyst nanoparticles on carbon black. *J Microsc* **232**, 248–259.
- GONTARD, L.C., DUNIN-BORKOWSKI, R.E., GASS, M.H., BLELOCH, A.L. & OZKAYA, D. (2009). Three-dimensional shapes and structures of lamellar-twinned fcc nanoparticles using ADF STEM. *J Electron Microsc* **58**, 167–174.
- GONTARD, L.C., OZKAYA, D. & DUNIN-BORKOWSKI, R.E. (2011). A simple algorithm for measuring particle size distributions on an uneven background from TEM images. *Ultramicroscopy* **111**, 101–106.
- GONZÁLEZ, J.C., HERNÁNDEZ, J.C., LÓPEZ-HARO, M., DEL RÍO, E., DELGADO, J.J., HUNGRIA, A.B., TRASOBARES, S., BERNAL, S., MIDGLEY, P.A. & CALVINO, J.J. (2009). 3D characterization of gold nanoparticles supported on heavy metal oxide catalysts by HAADF-STEM electron tomography. *Angew Chem Int Ed* **48**, 5313–5315.
- GUISBIERS, G., ABUDUKELIMU, G. & HOURLIER, D. (2011). Size-dependent catalytic and melting properties of platinum palladium nanoparticles. *Nanoscale Res Lett* **6**, 1–5.
- HANSEN, T.W., DELARIVA, A.T., CHALLA, S.R. & DATYE, A.K. (2013). Sintering of catalytic nanoparticles: Particle migration or Ostwald ripening? *ACC Chem Res* **46**(8), 1720–1730.
- HANSEN, T.W., WAGNER, T.W., HANSEN, P.L., DAHL, S., TOPSOE, H. & JACOBSEN, C.J.H. (2002). Atomic-resolution in-situ transmission electron microscopy of a promoter of a heterogeneous catalyst. *Science* **294**, 1508–1509.
- HARRIS, P.J.F. (1986). The sintering of platinum particles in an alumina-supported catalyst: Further transmission electron microscopy studies. *J Catal* **97**, 527–542.
- HARRIS, P.J.F. (1995). Growth and structure of supported metal catalyst particles. *Int Mater Rev* **40**(3), 97–115.

- HEIDENREICH, R.D., HESS, W.M. & BAN, L.L. (1968). A test object and criteria for high resolution electron microscopy. *J App Cryst* **1**, 1–19.
- HORCH, S., LORENSEN, F., HELVEG, S., LÆGSGAARD, E., STENSGAARD, I., JACOBSEN, K.W., NØRSKOV, J.K. & BESENBACHER, F. (1999). Enhancement of surface self-diffusion of platinum atoms by adsorbed hydrogen. *Nature* **398**, 134–136.
- JOSÉ-YACAMÁN, M., GUTIERREZ-WING, C., MIKI, M., YANG, D.-Q., PIYAKIS, K.N. & SACHER, E. (2005). Surface diffusion and coalescence of mobile metal nanoparticles. *J Phys Chem B* **109**, 9703–9711.
- KAMINO, T., KURODA, K. & SAKA, H. (1992). In situ HREM/microanalysis study of reduction of Al₂O₃ with palladium. *Ultramicroscopy* **41**, 245–248.
- KAMINO, T., YAGUCHI, T., KONNO, M., WATABE, A., MARUKAWA, T., MIMA, T., KURODA, K., SAKA, H., ARAI, S., MAKINO, H., SUZUKI, Y. & KISHITA, K. (2005). Development of a gas injection/specimen heating holder for use with transmission electron microscope. *J Electron Microsc* **54**(6), 497–503.
- KAMINO, T., YAGUCHI, T., SATO, T. & HASHIMOTO, T. (2005). Development of a technique for high resolution electron microscopic observation of nano-materials at elevated temperatures. *J Electron Microsc* **54**(6), 505–508.
- LINDEROTH, T.R., HORCH, S., LÆGSGAARD, E., STENSGAARD, I. & BESENBACHER, F. (1997). Surface diffusion of Pt on Pt(110): Arrhenius behavior of long jumps. *Phys Rev Lett* **78**(26), 4978–4981.
- MEHRAEEN, S., MCKEOWN, J.T., DESHMUKH, P.V., EVANS, J.E., ABELLAN, P., XU, P., REED, B.W., TAHERI, M.L., FISCHIONE, P.E. & BROWNING, N.D. (2013). A (S)TEM gas cell holder with localized laser heating for in-situ experiments. *Microsc Microanal* **19**, 470–478.
- MISHRA, Y.K., MOHAPATRA, S., AVASTHI, D.K., LALLA, N.P. & GUPTA, A. (2010). Tailoring the size of gold nanoparticles by electron beam inside transmission electron microscope. *Adv Mat Lett* **1**(2), 151–155.
- OZKAYA, D., THOMPSETT, D., GOODLET, G., SPRATT, S., ASH, P. & BOYD, D. (2003). Characterisation of C supported Pt nanoparticles using HREM. *Inst Phys Conf Ser* **179**, 127.
- PENG, Z., SOMODI, F., HELVEG, S., KISIELOWSKI, C., SPECHT, P. & BELL, A.T. (2012). High-resolution in-situ and ex situ TEM studies on graphene formation and growth on Pt nanoparticles. *J Catal* **286**, 22–29.
- RALPH, B.T.R. & HOGARTH, M.P. (2002). Catalysis for low-temperature fuel cells. Part I: The cathode challenges. *Plat Met Rev* **46**, 3–14.
- RUCKENSTEIN, E. & LEE, S.H. (1984). Redispersion and migration of Ni supported on alumina. *J Catal* **86**, 457.
- SANKARANARAYANAN, S.K.R.S., BHETHANABOTLA, V.R. & JOSEPH, B. (2005). Molecular dynamics simulation study of the melting of Pd-Pt nanoclusters. *Phys Rev B* **71**, 195415.
- SEPÚLVEDA-ESCRIBANO, A., COLOMA, F. & RODRÍGUEZ-REINOSO, F. (1998). Platinum catalysts supported on carbon blacks with different surface chemical properties. *Appl Catal A* **173**, 247–257.
- SIMONSEN, S.B., CHORKENDORFF, I., DAHL, S., SKOGLUNDH, M., SEHESTED, J. & HELVEG, S. (2010). Direct observations of oxygen-induced platinum nanoparticle ripening studied by in-situ tem. *J Am Chem Soc* **132**, 7968–7975.
- TAUSTER, S.J. (1987). Strong metal-support interactions. *J Am Chem Soc* **4**, 170–175.
- WYNBLATT, P. (1976). Particle growth in model supported metal catalysts-II. Comparison of experiment with theory. *Acta Metall* **24**, 1175–1182.
- WYNBLATT, P. & GJOSTEIN, N.A. (1976). Particle growth in model supported metal catalysts-I. Theory. *Acta Metall* **24**, 1165–1174.